EARTHQUAKE ENGINEERING AND STRUCTURAL DYNAMICS, VOL. 26, 215–231 (1997)

AN ANALYTICAL HYSTERESIS MODEL FOR ELASTOMERIC SEISMIC ISOLATION BEARINGS

MASARU KIKUCHI*

Izumi Research Institute, Shimizu Corporation, Fukoku Seimei Bldg. 2-2-2, Uchisaiwai-cho, Chiyoda-ku, Tokyo, 100, Japan

AND

IAN D. AIKEN*

Earthquake Engineering Research Center, University of California at Berkeley, 1301 South 46th St. Richmond, CA 94804, U.S.A.

SUMMARY

For the purpose of accurately predicting the seismic response of base-isolated structures, an analytical hysteresis model for elastomeric seismic isolation bearings is proposed. An extensive series of experimental tests of four types of seismic isolation bearings—two types of high-damping rubber bearings, one type of lead-rubber bearing and one type of silicon rubber bearing—was carried out with the objective of fully identifying their mechanical characteristics. The proposed model is capable of well-predicting the mechanical properties of each type of elastomeric bearing into the large strain range. Earthquake simulator tests were also conducted after the loading tests of the individual bearings. In order to show the validity of the proposed model, non-linear dynamic analyses were conducted to simulate the earthquake simulator test results. Good agreement between the experimental and analytical results shows that the model can be an effective numerical tool to predict not only the peak response value but also the force–displacement relationship of the isolators and floor response spectra for isolated structures.

KEY WORDS: elastomeric bearings; analytical model; seismic isolation; experiments; shake table

INTRODUCTION

Base isolation is a seismic design concept that affords a high level of protection to a structure from the damage caused by earthquakes. This is achieved by introducing some type of flexible support, usually at the foundation level, that moves the period of the structure away from the predominant period of the ground motion. Elastomeric bearings are now the most commonly used type of system for seismic isolation. The number of seismic isolation applications using elastomeric bearings has grown considerably in recent years.

The behaviour of a base-isolated structure is very similar to that of a single-degree-of-freedom system if the superstructure is rigid, and displacements are concentrated in the isolation bearings. The force–displacement relationship of typical elastomeric isolation bearings is non-linear as a result of their inherent damping properties. Therefore, the accurate prediction of the seismic behaviour of base-isolated structures depends strongly on the accuracy of the mathematical model of the non-linear mechanical properties of the isolation bearings.

Existing non-linear analytical models (bilinear or Ramberg–Osgood) have been applied for the dynamic analyses of base-isolated structures. However, experimentally obtained shear force–displacement relationships for elastomeric bearings show strong non-linearities and stiffening behaviour dependent on shear strain magnitude,[1] and it is not possible to represent such non-linear behaviour using any of the existing analytical models. For this reason a new analytical model has been developed.

* Research Engineer

CCC 0098–8847/97/020215–17

Received 12 December1995
Revised 8 August 1996

In this paper an analytical model for elastomeric seismic isolation bearings is proposed. It is shown to be suitable for four types of elastomeric seismic isolation bearings, and comparisons with experimental test results are presented. Two types of high-damping rubber bearings, one type of lead-rubber bearing and one type of silicon rubber bearing were studied. Tests of individual bearings and earthquake simulator tests of isolated structures were conducted for each type of bearing. The proposed analytical model is validated by comparison of analytical results with the measured experimental results.

AN ANALYTICAL MODEL FOR ELASTOMERIC BEARINGS

Before a description of the proposed model is presented, existing non-linear models for isolation bearings are discussed. Both the bilinear and Ramberg–Osgood models have been used to model the force–displacement relationship for elastomeric isolation bearings. These models have also been modified to include the procedure of updating parameters during the analysis. Both of these models assume bearing damping to be hysteretic in nature. Both models define a skeleton curve and hysteresis loops separately. The skeleton curve is defined by the following relationship:

$$F = K_{\text{eff}} X \tag{1}$$

where F is the shear force, X is the shear displacement and K_{eff} is the effective shear stiffness of the bearing. K_{eff} is typically evaluated using an empirical formula for elastomer shear modulus as a function of shear strain. This relationship is typically determined from shear tests of bearings, assuming:

$$K_{\text{eff}} = \frac{G(\gamma)A}{H_{\text{r}}} \quad \text{and} \quad \gamma = \frac{\delta_{\text{h}}}{H_{\text{r}}} \tag{2}$$

where $G(\gamma)$ is the elastomer shear modulus as a function of shear strain, γ is the shear strain, A is the bearing shear area, H_{r} is the total height of rubber in the bearing, and δ_{h} is the relative horizontal displacement between the top and bottom ends of the bearing.

Experimentally observed stiffness and damping functions for elastomeric bearings have been described in terms of shear strain because these properties are strongly related to the shear strain magnitude. These models thus involve the procedure of updating their parameters to specify the shape of the hysteresis curve according to the maximum shear strain at the point of unloading from the skeleton curve. The parameters are evaluated so that the stiffness and damping of the analytical model are equivalent to the values from the empirical formulae. This procedure is reasonable, considering the unique mechanical properties of elastomeric bearings. The bilinear and Ramberg–Osgood models are suitable for low-to-moderate levels of shear strain. However, neither model adequately captures the high-strain behaviour of elastomeric bearings, when the bearings exhibit strong non-linear stiffening.

In addition to the modified bilinear model and the modified Ramberg–Osgood model, differential equation models, such as the Ozdemir model,[2] or the Wen model[3] have been proposed. These models have been used to predict the behaviour of various types of seismic isolation devices and energy dissipators (e.g. References 4 and 5). In these models, the parameters that control the shape of the hysteresis loop are constant and they must be determined at the beginning of the analysis. Fujita *et al.*[6] improved upon the Ozdemir model by including a procedure to update parameters, along the lines of the modified bilinear model and the modified Ramberg–Osgood model.

After the above-mentioned assessment of existing models, the following equations (3)–(5) were found to successfully model the behaviour of elastomeric bearings into the large strain range. Equations (3)–(5) were derived by modifying the Fujita model in order to improve the performance of the model at high shear strain levels. The proposed model neglects the effects of strain rate and variation of axial load on the bearing hysteresis properties:

$$F = F_1 + F_2 \tag{3}$$

$$F_1 = \tfrac{1}{2}(1 - u)F_m\{x + \text{sgn}(X)|x|^n\} \tag{4}$$

$$F_2 = uF_m\{1 - 2e^{-a(1+x)} + b(1+x)e^{-c(1+x)}\}, \quad (\dot{X} > 0)$$
$$F_2 = -uF_m\{1 - 2e^{-a(1-x)} + b(1-x)e^{-c(1-x)}\}, \quad (\dot{X} < 0) \tag{5}$$

where F_m is the peak shear force on the skeleton curve, x is the normalized shear displacement ($x = X/X_m$) and X_m is the peak shear displacement on the skeleton curve. In equation (4), the parameter n specifies the stiffening. In equation (5), u is the ratio of shear force at zero displacement, F_u, to $F_m(u = F_u/F_m)$, a is calculated from equation (6) and b is calculated from equation (7). Both equations (6) and (7) are derived assuming that the analytical and experimental hysteresis loop areas are equal:

$$\frac{1 - e^{-2a}}{a} = \frac{2u - \pi h_{eq}}{2u} \tag{6}$$

$$b = c^2\left[\frac{\pi h_{eq}}{u} - \left\{2 + \frac{2}{a}(e^{-2a} - 1)\right\}\right] \tag{7}$$

where h_{eq} is the equivalent viscous damping ratio and is evaluated from an empirical formula as a function of shear strain, which is determined from the results of tests of individual bearings. The parameter c is a preselected constant which specifies the shape of the hysteresis loop. Equation (6) cannot be solved in closed form for a and thus must be solved numerically. All of the parameters that control the shape of the hysteresis loop are updated using equations (6) and (7) when load reversal occurs from the skeleton curve, expressed by equation (1). Figure 1 shows typical hysteresis loops given by equations (3)–(5). Figure 1(a) was obtained by substituting $b = 0$ in equation (5). The shape of the hysteresis loop in Figure 1(a) is typical of that at low-to-moderate shear strain levels. The non-linear stiffening behaviour at displacements corresponding to high shear strains in the elastomer can be represented by calibrating the parameters b and c in equation (5), such as shown in Figure 1(b). The model expressed by equations (3)–(5) can easily capture the feature of the smooth transition of the hysteresis loops from the low to high shear strain levels.

The above formulae are derived for application to steady-state hysteresis behaviour for elastomeric bearings. It is necessary to further develop a hysteresis rule for the randomly varying displacement conditions of earthquake response analyses. Masing rule is applied to fully define the bearing shear force under a randomly-varying displacement,[7] and equation (5) is replaced by equation (8) below:

$$F_2 = \begin{cases} F_{2i} + uF_m\{2 - 2e^{-a(x-x_i)} + b(x-x_i)e^{-c(x-x_i)}\}, & (\dot{X} > 0) \\ F_{2i} - uF_m\{2 - 2e^{a(x-x_i)} - b(x-x_i)e^{c(x-x_i)}\}, & (\dot{X} < 0) \end{cases} \tag{8}$$

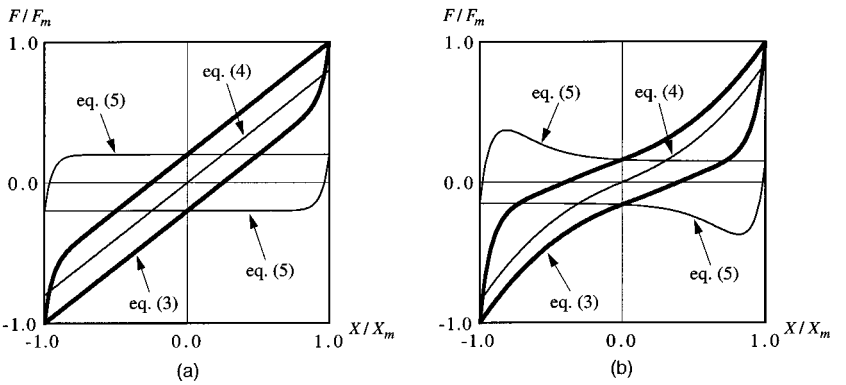

Figure 1. Normalized hysteresis loops: (a) low shear strain level; (b) high shear strain level

where

$$F_{2i} = F_i - F_1$$

$$x_i = \frac{X_i}{X_m}$$

and (X_i, F_i) is the most recent point of load reversal.

When the load reversal occurs in the same region, i.e. $X_i \cdot X_{i-1} > 0$ (X_{i-1} is the reversal displacement at the step before X_i), equation (8) should be replaced by equation (9) to avoid excessive enlargement of the hysteresis loop at load reversal in the stiffening range:

$$F_2 = \begin{cases} F_{2i} + \alpha_1 u F_m \{2 - 2e^{-a(x - x_i)}\}, & (\dot{X} > 0) \\ F_{2i} - \alpha_2 u F_m \{2 - 2e^{a(x - x_i)}\}, & (\dot{X} < 0) \end{cases} \tag{9}$$

where

$$\alpha_1 = \frac{2 - 2e^{a(x_i - x_{i-1})} - b(x_i - x_{i-1})e^{c(x_i - x_{i-1})}}{2 - 2e^{a(x_i - x_{i-1})}}$$

$$\alpha_2 = \frac{2 - 2e^{-a(x_i - x_{i-1})} + b(x_i - x_{i-1})e^{-c(x_i - x_{i-1})}}{2 - 2e^{-a(x_i - x_{i-1})}}$$

It is known that the mechanical properties of elastomeric bearings are affected by load history. When a bearing experiences a high shear strain deformation, the subsequent stiffness in the small strain range is somewhat degraded compared to the virgin-state small strain stiffness.[8] Moreover, the stiffness gradually degrades with repeated cycling at the same displacement amplitude. It is recognized as a complex phenomenon. In the bearing test results described in References 9 and 10, the most significant differences are seen between the stiffness of the first cycle and of subsequent cycles. A reasonable method to represent this phenomenon is to introduce two stages of effective stiffness for the skeleton curve, as expressed by equation (1). Therefore, the additional force given by equation (10) should be added to the bearing shear force given by equation (1):

$$\begin{aligned} &\Delta F = (K_{\text{eff},i} - K_{\text{eff}})X \quad (X < X_{\min} \text{ or } X > X_{\max}) \\ &\Delta F = 0 \quad (X_{\min} < X < X_{\max}) \end{aligned} \tag{10}$$

where $X_{\max}$ and $X_{\min}$ are the maximum and minimum values of experienced displacement, $K_{\text{eff},i}$ is the effective shear modulus of the elastomer obtained from a first-loading test of a bearing (i.e. without any prior load history). In contrast, K_{eff} in equation (1) should be obtained from a test that includes load history (i.e. from the second or later cycle). When $X_{\max}$ or $X_{\min}$ is updated ΔF should be increased gradually so that a smooth transition between the two forms of equation (10) is achieved (Figure 2).

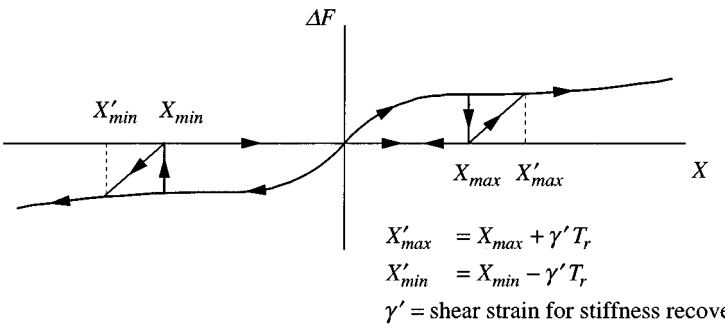

Figure 2. Hysteresis rule for stiffness degradation associated with load history

VERIFICATION OF PROPOSED MODEL

Application 1

Earthquake simulator tests of a 1/2·5-scale model of an existing base-isolated, three-storey reinforced-concrete building in Japan were conducted.[11] The main objectives of the study were to fully identify the mechanical characteristics of three types of isolation bearings, to investigate the response of the large-scale model on each of the three systems under design-level motions, and to subject the isolated model to ultimate-level earthquake shaking, investigating the interaction between stiffening of the isolators and inelastic action in the concrete superstructure.

Two types of high-damping rubber bearing and one type of lead-rubber bearing were used in these tests (Figure 3). The high-damping A bearings were made from a blend of filled natural rubber and synthetic rubber. The bearings consisted of 20 layers of 2·2 mm thick rubber at 176 mm diameter (shape factor = 20), 19 1·0 mm steel shims, and 12 mm top and bottom plates. The bearings were designed with flange-type end plates to permit bolted structure and foundation connections. The high-damping B bearings were made from a low-modulus, filled natural rubber compound. The bearings consisted of 12 layers of 4·0 mm thick rubber at 140 mm diameter (shape factor = 8·75), 11 1·6 mm steel shims, and 20 mm top and bottom plates. Bearing-structure and foundation connections were bolted. Instead of using flange-type end plates, however, the high-damping B bearings were connected by bolting directly into top and bottom end plates. The lead-rubber bearings were made from an unfilled natural rubber compound, and contained a 25 mm diameter lead plug. The bearings consisted of 21 layers of 3·0 mm thick rubber at 180 mm diameter (shape factor = 15), 20 1·0 mm steel shims, and 15 mm top and bottom plates. The bearings had shear dowel end plate connections.

Before the earthquake simulator tests were conducted, tests of individual bearings were performed. A detailed description of these tests is provided in Reference 9. Typical hysteresis loops for the three types of bearings under sinusoidal shear displacement loading are presented in Figure 4. The loops shown for the high-damping A bearing are at shear strains from 5 to 350 per cent, for the high-damping B bearing from 5 to 250 per cent, and for the lead-rubber bearing from 5 to 200 per cent. Beyond a certain strain level the high-damping bearings exhibit a clear stiffening behaviour. This stiffening is a material property of filled rubbers. The lead-rubber bearing, which was made from unfilled rubber and had doweled shear connections, did not show the large-strain stiffening effect.

In order to apply the proposed model to these isolation bearings, empirical formulae as functions of shear strain were carefully identified from the test results using the least-squares method. The formulae obtained

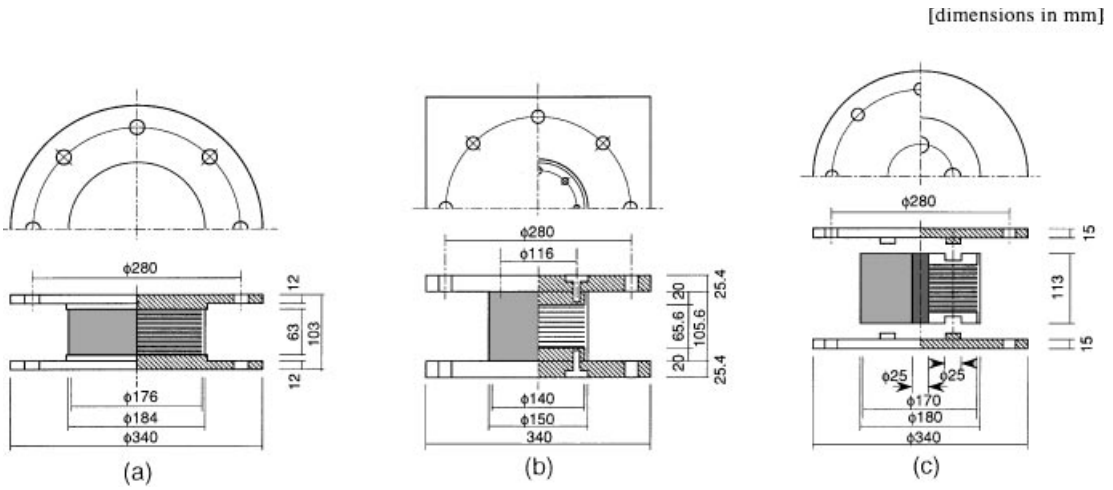

Figure 3. Elastomeric isolation bearings used in the earthquake simulator tests: (a) high-damping A; (b) high-damping B; (c) lead-rubber

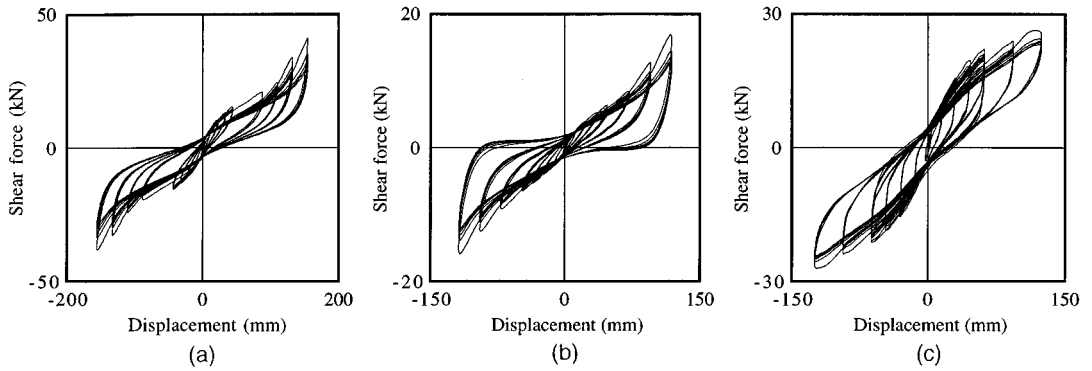

Figure 4. Shear force–displacement hysteresis loops obtained from tests of individual bearings: (a) high-damping A; (b) high-damping B; (c) lead-rubber

are summarized in Table I. Figure 5 shows the analytically obtained hysteresis loops under the same displacements histories as the experimental hysteresis loops shown in Figure 4. Good results were obtained for all three types of bearings. The proposed model can accurately predict the force–displacement relationship into the large strain range.

After the tests of individual bearings the earthquake simulator tests were conducted. The test structure shown in Figure 6 was designed and constructed to be a 1/2·5-scale model of an existing three-storey, reinforced-concrete base-isolated building. Member stiffnesses and yield strengths were carefully scaled, and the concrete mix designed to match the strength of the concrete in the full-size building as accurately as possible. The floor weights of the model were uniform, with a total model weight of 40·8 t. The model was isolated on six bearings, and foundation details permitted the bearings to be easily changed. The model was designed to include detachable bracing. The main purpose of the bracing was to ensure that no damage occurred during the design-level tests with the different isolation systems. This permitted direct comparisons between the three systems. The model was not braced in the ultimate-level tests.

The design-level earthquake test program investigated the performance of the isolated braced model with earthquake intensities specified by the Japanese seismic code. The earthquakes used were the 1940 El Centro (N–S), 1968 Hachinohe (N–S), and 1978 Miyagi (N–S) records. Each of these motions was input at two intensities, corresponding to peak velocities of 25 and 50 cm/s for the prototype structure. These velocities are the two design levels specified by the Japanese seismic design code for conventional buildings.[12] For the ultimate-level earthquake tests the bracing was removed and the model isolated on the high-damping A bearings was subjected to two large-intensity motions. The two motions were Miyagi, with a PGA of 0·77g, and the SCT station recording of the 1985 Michoacan earthquake, with a PGA of 0·48g. The corresponding full-scale peak velocities for these two inputs were 70 and 60 cm/s, respectively. The SCT motion is particularly severe for isolation systems because it has a very-well defined spectral peak at 2 s, almost exactly at the design period for many isolation systems. In the case of the model on the high-damping A system, the SCT motion represented essentially a resonance excitation. A detailed description of the test results is provided in Reference 11.

In order to simulate the earthquake simulator test results, dynamic response analyses were conducted using the previously proposed hysteresis model for elastomeric bearings. The test structure was modelled as a 2D planar frame (Figure 7) with all out-of-plane degrees of freedom constrained to zero. Mass is concentrated at each node. The structural frame was modelled using frame (beam-column) elements with two concentrated flexural springs at the ends which permitted inelastic deformation of the members.[13] The Takeda model was used for the flexural springs.[14] The bracing used in the design-level earthquake tests was modelled using linear truss elements. The isolation bearings were modelled using two spring elements; a non-linear shear spring and a linear axial spring. The proposed hysteresis model was used for the shear spring hysteresis properties. Stiffness proportional damping was applied only to the superstructure.

Table I. Empirical formulae for high-damping A, high-damping B and lead-rubber bearing models (γ: shear strain)

High-damping A	High-damping B	Lead-rubber
$K_{\text{eff}} = 351\,\gamma^{-0.461}$ ($\gamma \leqslant 1.0$) (N/mm)	$K_{\text{eff}} = 116\,\gamma^{-0.295}$ ($\gamma \leqslant 1.2$) (N/mm)	$K_{\text{eff}} = 337\,\gamma^{-0.346}$ ($\gamma \leqslant 0.75$) (N/mm)
$= 510 - 195\gamma + 34.7\gamma^2$ ($\gamma > 1.0$)	$= 144 - 40.4\gamma + 9.79\gamma^2$ ($\gamma > 1.2$)	$= 558 - 291\gamma + 54.1\gamma^2$ ($\gamma > 0.75$)
$K_{\text{eff},i} = 378\,\gamma^{-0.460}$ ($\gamma \leqslant 1.0$) (N/mm)	$K_{\text{eff},i} = 124\,\gamma^{-0.282}$ ($\gamma \leqslant 1.2$) (N/mm)	$K_{\text{eff},i} = 366\,\gamma^{-0.302}$ ($\gamma \leqslant 0.75$) (N/mm)
$= 563 - 232\gamma + 44.6\gamma^2$ ($\gamma > 1.0$)	$= 154 - 49.7\gamma + 15.8\gamma^2$ ($\gamma > 1.2$)	$= 590 - 293\gamma + 51.3\gamma^2$ ($\gamma > 0.75$)
$h_{\text{eq}} = 0.123 - 0.00876\gamma$	$h_{\text{eq}} = 0.101 - 0.0191\gamma + 0.0143\gamma^2$	$h_{\text{eq}} = 0.202 - 0.0457\gamma$
$u = 0.221 - 0.0344\gamma$	$u = 0.191 - 0.0287\gamma$	$u = 0.384 - 0.288\gamma + 0.0748\gamma^2$
$n = 1.0$ ($\gamma \leqslant 2.0$)	$n = 1.0$ ($\gamma \leqslant 1.5$)	$n = 1.0$ (const.)
$= -1.96 + 1.48\gamma$ ($\gamma > 2.0$)	$= 3.60 - 3.48\gamma + 1.17\gamma^2$ ($\gamma > 1.5$)	a: obtained from equation (6)
a: obtained from equation (6)	a: obtained from equation (6)	if $a > 14.0$, $a = 14.0$ (const.)
if $a > 15.2$, $a = 15.2$ (const.)	if $a > 13.0$, $a = 13.0$ (const.)	b: obtained from equation (7)
b: obtained from equation (7)	b: obtained from equation (7)	if $\gamma \leqslant 0.25$, $b = 0.0$ (const.)
if $\gamma \leqslant 0.75$, $b = 0.0$ (const.)	if $\gamma \leqslant 1.0$, $b = 0.0$ (const.)	$c = 4.0$ (const.)
$c = 6.0$ (const.)	$c = 6.0$ (const.)	

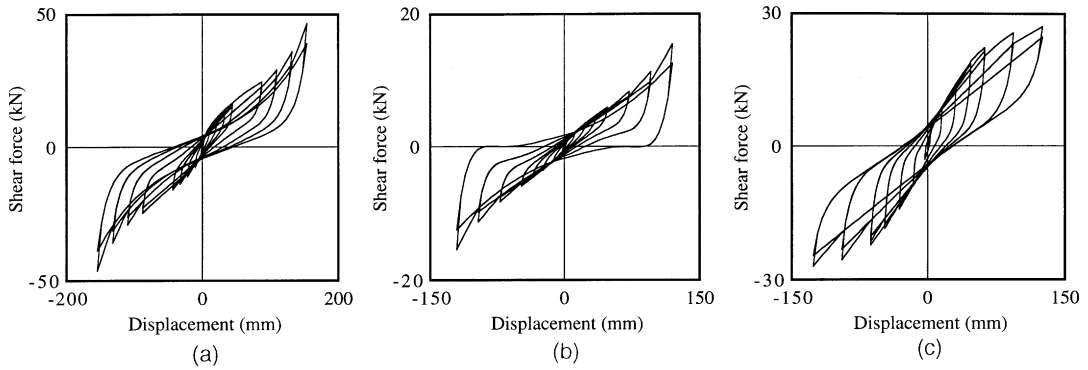

Figure 5. Shear force–displacement hysteresis loops obtained from analyses of tests of individual bearings: (a) high-damping A; (b) high-damping B; (c) lead-rubber

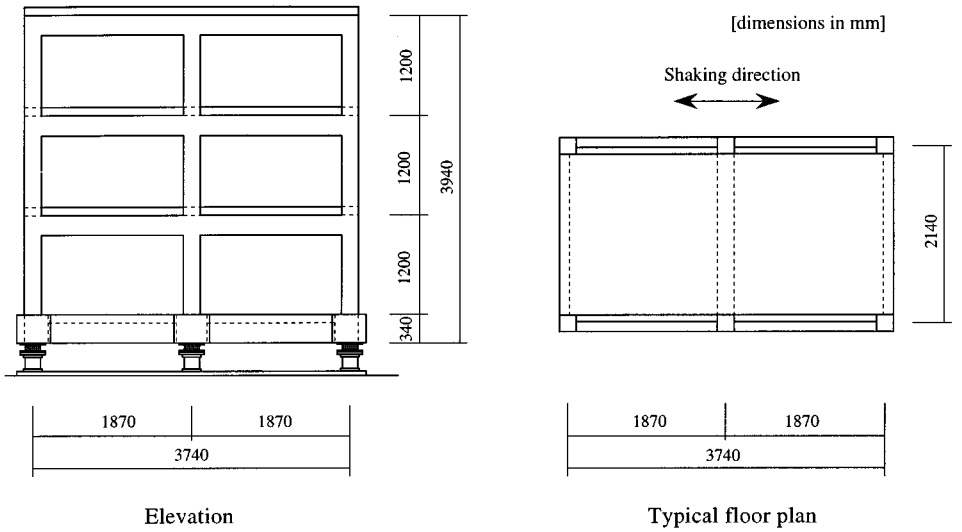

Figure 6. 1/2·5-scale model of isolated building

A damping ratio of 5 per cent of critical was defined for the fundamental period of the fixed-base structure.

The dynamic response analyses were conducted in the same sequence as the earthquake simulator tests. All of the analyses were performed using the experimentally observed shake table response signals as the input for the analyses. Step-by-step direct time integration was performed assuming constant average acceleration and a time increment of 0·005 s, which was the same as the data sampling interval for the earthquake simulator tests.

Analytical and experimental results for the braced model are presented in Table II and Figures 8–10. Table II summarizes the experimental and analytical peak response values, listing peak roof acceleration, peak bearing displacement, and the difference between the experimental and analytical results as a percentage of the experimental result. Analytical peak response quantities are all within 20 per cent of the experimental values. Figures 8 and 9 present a comparison of the three isolation system hysteresis loops for the El Centro $V_{max} = 50$ cm/s input. The analytical hysteresis loops for the high-damping A system show good agreement with the experimental observations, and neither response shows any stiffening at large

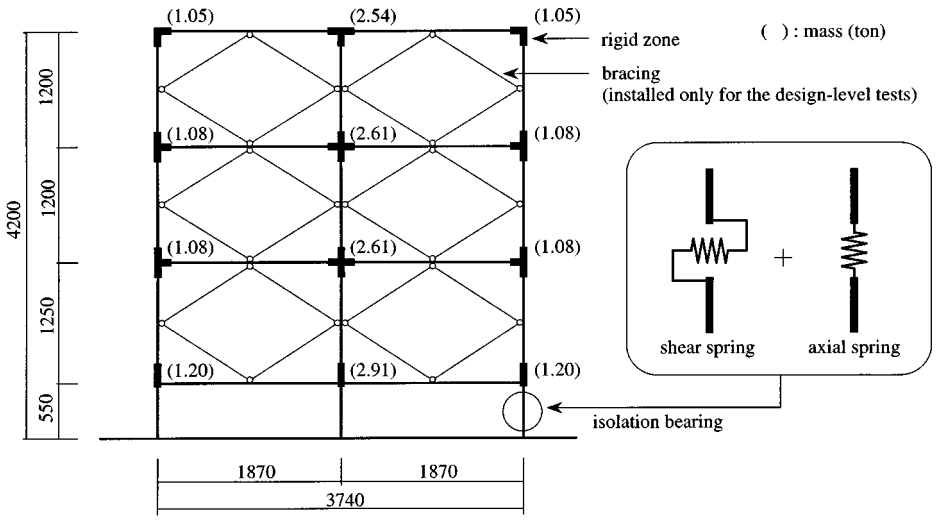

Figure 7. 2D planar frame model for analyses

Table II. Comparison of peak response values, Application 1

Isolation system	Signal	V_{max} (cm/s)	Roof acc. (gal)			Bearing displ. (mm)		
			Exp.	Ana.	Ana./Exp.	Exp.	Ana.	Ana./Exp.
High-damping A	El Centro	25	189	203	1·07	26·5	28·8	1·09
	Hachinohe		186	212	1·14	24·6	26·1	1·06
	Miyagi		263	241	0·92	41·1	40·6	0·99
	El Centro	50	289	313	1·08	48·0	55·5	1·16
	Hachinohe		294	334	1·14	54·0	61·5	1·14
	Miyagi		456	416	0·91	85·6	88·7	1·04
High-damping B	El Centro	25	129	119	0·92	60·2	62·6	1·04
	Hachinohe		152	128	0·84	75·2	70·9	0·94
	Miyagi		86·8	76·8	0·88	38·1	38·3	1·01
	El Centro	50	208	208	1·00	114	103	0·90
	Hachinohe		195	231	1·18	126	119	0·94
	Miyagi		151	153	1·01	78·4	83·4	1·06
Lead-rubber	El Centro	25	167	175	1·05	19·0	20·1	1·06
	Hachinohe		163	195	1·20	21·5	22·8	1·06
	Miyagi		243	222	0·91	31·9	29·1	0·91
	El Centro	50	289	322	1·11	39·6	42·4	1·07
	Hachinohe		295	342	1·16	44·9	49·7	1·11
	Miyagi		439	417	0·95	74·4	80·1	1·08

deformations (Figures 8(a) and 9(a)). The experimental result for the high-damping B system exhibits slight stiffening behaviour (Figure 8(b)), which is captured accurately by the analysis (Figure 9(b)). The shape of the experimentally observed hysteresis loops for the lead-rubber system is very similar to typical bilinear behavior (Figure 8(c)). This behaviour is also well-captured by the proposed model (Figure 9(c)). In general, good correlation between the experimental and anlytical results was obtained for all three isolation systems.

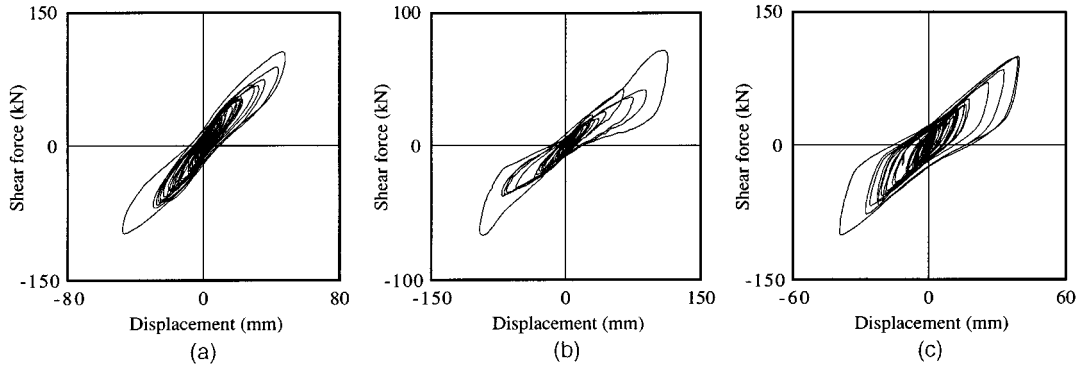

Figure 8. Experimentally observed isolation system hysteresis for braced model and El Centro $V_{max} = 50$ cm/s input: (a) high-damping A; (b) high-damping B; (c) lead-rubber

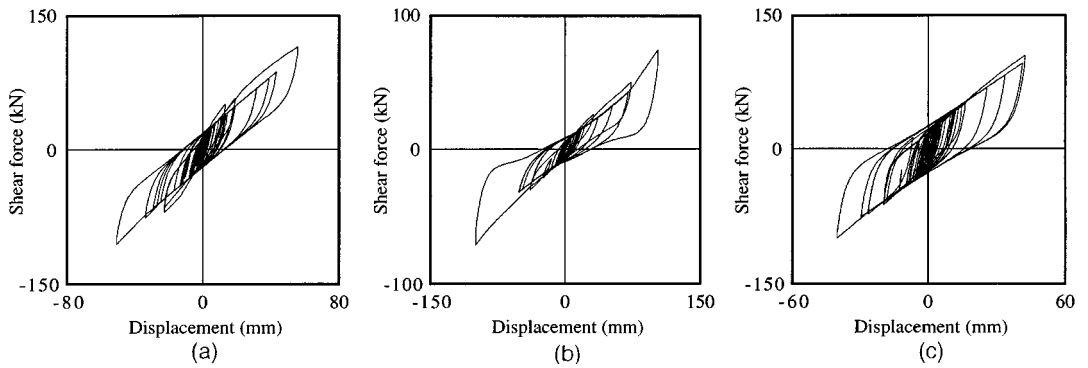

Figure 9. Analytically obtained isolation system hysteresis for braced model and El Centro $V_{max} = 50$ cm/s input: (a) high-damping A; (b) high-damping B; (c) lead-rubber

Five per cent-damped response spectra for each isolation system are presented in Figure 10. The response spectra were calculated from experimentally observed and analytically obtained response accelerations at the roof level of the braced model for the El Centro $V_{max} = 50$ cm/s input. The experimental and analytical spectra are very similar over a wide period range.

Figures 11 and 12 present the experimental and analytical interstory drift versus storey shear force relationships for the unbraced model on the high-damping A isolation system for the SCT $V_{max} = 60$ cm/s input. In this test the isolation bearings deformed sufficiently to reach the high-strain stiffening range. Stiffening of the bearings subjected the superstructure to significant shear demands; in fact, the level of lateral force induced in the superstructure in this test was approximately the lateral capacity of the building. This was confirmed by the extensive inelastic action throughout the superstructure that was recorded by rebar strain gauges. (It should be noted that the experimental intent of this test was to subject the isolated structure to a beyond worst-case earthquake motion – the very soft soil SCT motion represented a pseudo-resonant excitation, and was input at a significantly increased intensity.) The analysis captured the behaviour at each storey quite accurately, and the stiffening behaviour in the isolation bearings was well represented. Figure 13 shows the extent of yielding observed in the superstructure and Figure 14 shows the peak ductility ratios obtained by analysis. The figures indicate good correlation between the experimentally observed yielding locations and the plastic hinge locations predicted by analysis.

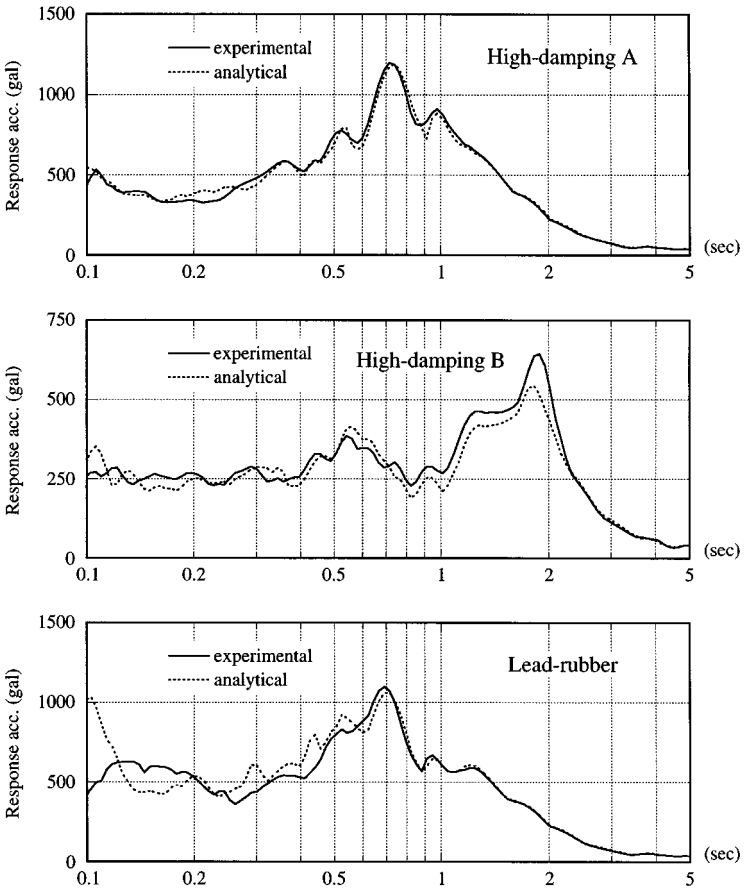

Figure 10. Five per cent-damped response spectra for roof level of braced model and El Centro $V_{max} = 50$ cm/s input

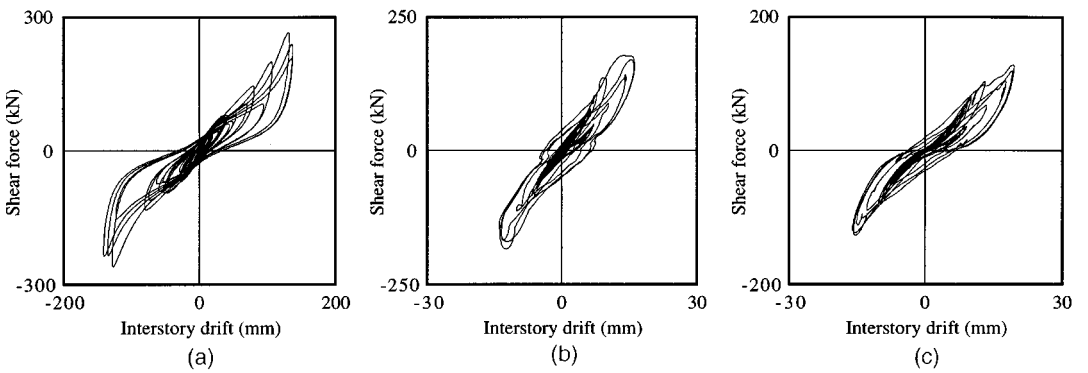

Figure 11. Experimentally observed storey shear force versus interstory drift relationships for unbraced model and SCT $V_{max} = 60$ cm/s input: (a) isolation level; (b) first storey; (c) second storey

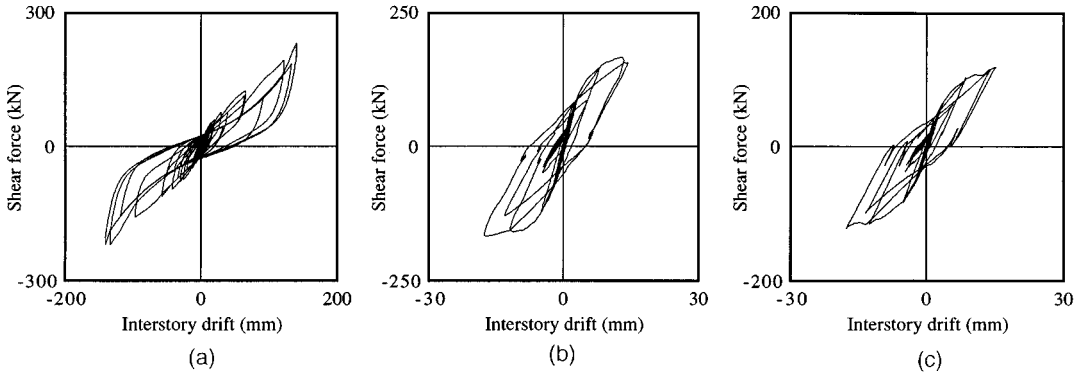

Figure 12. Analytically obtained storey shear versus interstory drift relationships for unbraced model and SCT $V_{max} = 60$ cm/s input: (a) isolation level; (b) first storey; (c) second storey

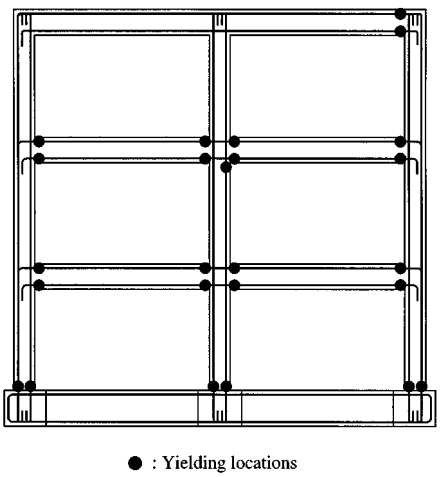

Figure 13. Experimentally observed locations of yielding in model for SCT $V_{max} = 60$ cm/s input

Application 2

Earthquake simulator tests were conducted to show the validity of a new base isolation system for seismic protection and vibration isolation. The system uses silicon rubber, which was developed to provide a lower shear modulus for isolation bearings than typically offered by other existing types of elastomers suitable for seismic isolation. The silicon rubber bearings were made from a blend of filled natural rubber and silicon rubber. The bearings were designed with flange-type end plates to permit bolted structure and foundation connections. The bearings consisted of 27 layers of 1·0 mm thick silicon rubber at 120 mm diameter (shape factor = 30), 26 1·0 mm steel shims and 10 mm top and bottom plates (Figure 15). Before the earthquake simulator tests were conducted tests of individual bearings were performed. Typical hysteresis loops for a silicon rubber bearing under sinusoidal shear displacement loading are shown in Figure 16. The loops shown are for shear strains from 25 to 200 per cent. The hysteresis loops are similar in shape to those for the high-damping A bearing presented previously. Stiffening behaviour is seen beyond about 150 per cent shear strain. The effect of load history on elastomer properties is much smaller than with the high-damping A elastomer.

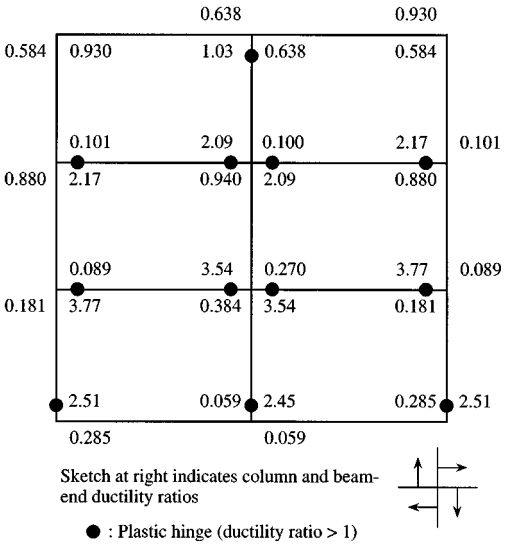

Figure 14. Analytically obtained peak ductility ratios in model for SCT $V_{max} = 60$ cm/s input

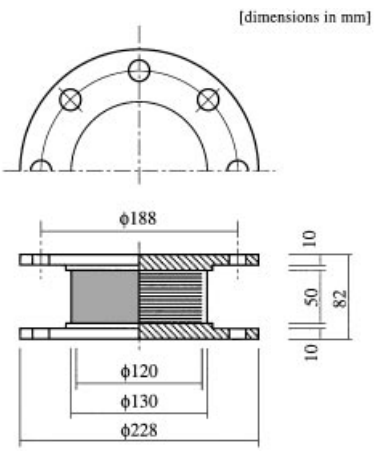

Figure 15. Silicon rubber bearing used in the earthquake simulator tests

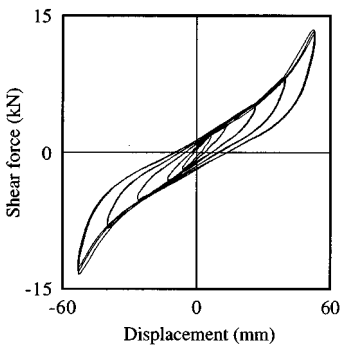

Figure 16. Shear force–displacement hysteresis loops obtained from tests of individual silicon rubber bearing

Empirical formulae for the silicon rubber bearing are summarized in Table III. These were identified from the tests of individual bearings in the same way as for the three bearing types described in Application 1. Figure 17 shows hysteresis loops obtained from analysis for the same shear displacement loading history as for the experimental results shown in Figure 16. Excellent correlation is obtained between the experimental and analytical results.

After the individual bearing tests earthquake simulator tests were conducted. The test structure shown in Figure 18 was designed and constructed to be a 0·24-scale model of a full-scale system with isolation bearings each supporting 28·7 kN. The model consisted of a steel frame with precast concrete weights for added mass. It has a total weight of 11·7 t and was isolated on four bearings.

Vibration and earthquake simulator tests were carried out to quantify the effectiveness of the isolation system in different configurations. The testing consisted of two programs. The first test program investigated the performance of the bearings for isolation against traffic-induced vibrations. Accelerations recorded on the ground near a railroad were used as the input vibrations. The second program investigated the performance of the isolation system to earthquake ground motions with intensities specified by the Japanese seismic code. The earthquake motions used were the 1940 El Centro (N–S), 1952 Taft (E–W) and 1968 Hachinohe (N–S) records. Each of these motions was input at two intensities, corresponding to the design-level velocities of 25 and 50 cm/s for the full-scale structure. A detailed description of the test results is provided in Reference 15.

Dynamic response analyses of the earthquake simulator tests were conducted using the previously proposed hysteresis model. The test structure was modelled as a single-degree-of-freedom system (Figure 19),

Table III. Empirical formulae for silicon rubber bearing model (γ: shear strain)

$K_{\text{eff}} = 174\gamma^{-0\cdot441}$ ($\gamma \leqslant 0\cdot483$) (N/mm)
$= 307 - 189\gamma + 81\cdot3\gamma^2$ ($\gamma > 0\cdot483$)
$K_{\text{eff},i} = 182\gamma^{-0\cdot397}$ ($\gamma \leqslant 0\cdot495$) (N/mm)
$= 326 - 217\gamma + 92\cdot2\gamma^2$ ($\gamma > 0\cdot495$)
$h_{\text{eq}} = 0\cdot112 + 0\cdot0129\gamma - 0\cdot0138\gamma^2$
$u = 0\cdot260 - 0\cdot070\gamma$
$n = 1\cdot0$ ($\gamma \leqslant 1\cdot0$)
$= 2\cdot99 - 3\cdot84\gamma + 1\cdot85\gamma^2$ ($\gamma > 1\cdot0$)
a: obtained from equation (6)
if $a > 12\cdot8$, $a = 12\cdot8$ (const.)
b: obtained from equation (7)
if $\gamma \leqslant 1\cdot0$, $b = 0\cdot0$ (const.)
$c = 7\cdot0$ (const.)

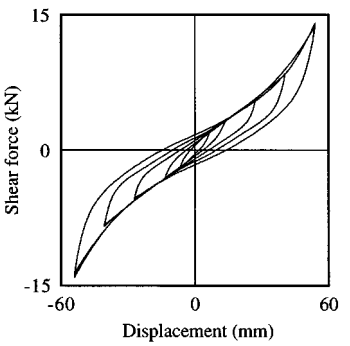

Figure 17. Shear force–displacement hysteresis loops obtained from analyses of tests of individual silicon rubber bearing

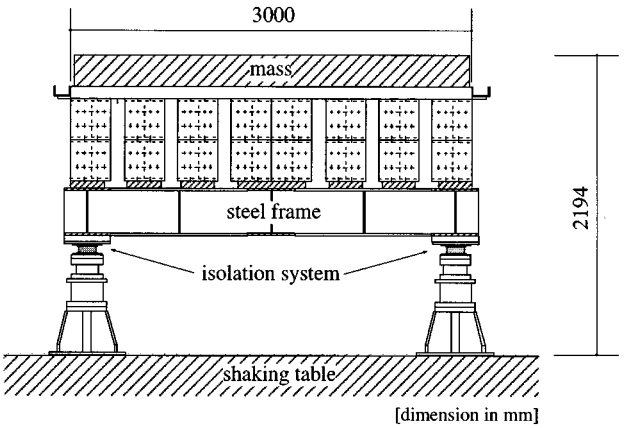

Figure 18. Test structure for silicon rubber bearing isolation system

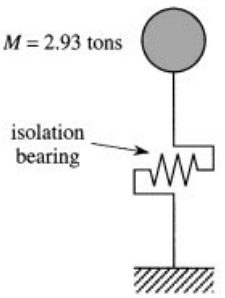

Figure 19. Single-degree-of-freedom system for analyses

Table IV. Comparison of peak response values for silicon rubber isolation system earthquake simulator tests

Signal	V_{max} (cm/s)	Acc. (gal)			Displ. (m)		
		Exp.	Ana.	Ana./Exp.	Exp.	Ana.	Ana./Exp.
El Centro	25	127	127	1·00	17·1	16·9	0·99
Taft		128	118	0·92	18·1	15·3	0·85
Hachinohe		99·4	107	1·08	12·9	13·5	1·06
El Centro	50	326	329	1·01	45·0	44·6	0·99
Taft		335	276	0·82	45·9	39·6	0·86
Hachinohe		163	178	1·09	25·2	26·1	1·04

which represented one-quarter of the structure, considering symmetry. The proposed elastomeric bearing hysteresis model was used for the shear spring. All of the analyses were performed using the measured shake table response as input.

Analytical and experimental results for the model are presented in Table IV and Figures 20 and 21. Table IV summarizes the experimental and analytical peak response values, listing the peak model

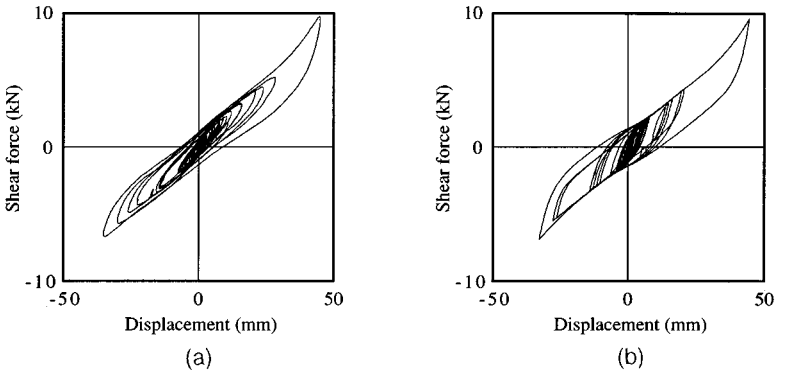

Figure 20. Silicon rubber isolation system hysteresis loops for El Centro $V_{max} = 50$ cm/s input: (a) experimental; (b) analytical

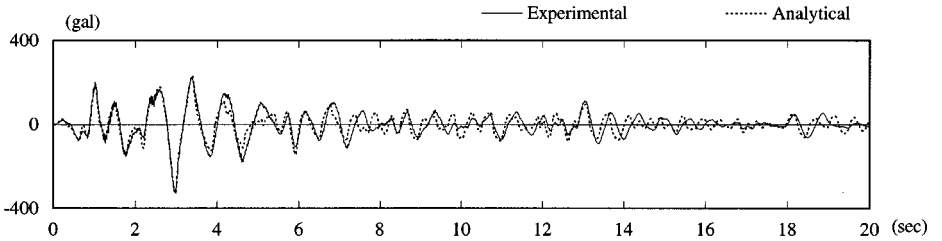

Figure 21. Silicon rubber isolation system experimental and analytical response acceleration time histories for El Centro $V_{max} = 50$ cm/s input

acceleration, peak bearing displacement and the difference between the experimental and analytical results as a percentage of the experimental value. Peak response values for the El Centro and Hachinohe inputs were predicted to within 9 per cent of the experimental results. The analysis results for the Taft tests varied by up to 18 per cent, more than for any of the other earthquake motions. Figure 20 presents a comparison of the isolation system hysteresis loops for the El Centro $V_{max} = 50$ cm/s input. It can be seen that the analytical model captures the actual behaviour into the stiffening range very well. Figure 21 compares the model response acceleration time history for the El Centro $V_{max} = 50$ cm/s input. Good correlation can be seen between the observed and predicted results.

CONCLUSIONS

An analytical hysteresis model for elastomeric seismic isolation bearings has been presented for the purpose of accurately predicting the seismic response of base-isolated structures. The analytical model is based on the strong shear strain-dependent non-linearities of elastomeric isolation bearings. The model requires careful identification of the parameters specifying the shape of hysteresis loops obtained from dynamic loading tests of individual bearings. The application to four different types of seismic isolation bearings — two types of high-damping rubber bearings, one type of lead-rubber bearing, and one type rubber bearing — is presented.

The validity of the model was demonstrated with dynamic analyses of two isolated structures and comparisons with earthquake simulator test results. Good agreement between the analytical and experimental results was obtained, not only for peak response values, but also for the isolator force–displacement relationships, response acceleration time histories and floor response spectra. These results provide the confidence necessary to use the proposed model for the design of base-isolated structures.

The analytical model and methodology presented in this paper are based upon establishing empirical model parameters by matching of actual bearing test results. Further work to develop analytical models of elastomeric bearings, and particularly of high-damping rubber bearings, based upon fundamental principles of computational continuum mechanics is required.

ACKNOWLEDGEMENTS

The earthquake simulator tests described in Application 1 were undertaken as part of a joint research project on base isolation between Shimizu Corporation, Tokyo, Japan and the Earthquake Engineering Research Center of the University of California at Berkeley, U.S.A. The authors would like to express their thanks to Dr. Peter W. Clark, Dr. James M. Kelly, Mr. Masaaki Saruta and Dr. Kazuo Tamura. The silicon rubber bearings described in Application 2 were developed under a joint research project involving Shimizu Corporation, Bridgestone Corporation, Japan and Shinetsu Chemical Industry Corporation, Japan. The authors would also like to express their thanks to Mr. Shoji Hayashi, Mr. Toshikazu Yoshizawa and Mr. Ken Fukuda.

REFERENCES

1. J. M. Kelly, 'Dynamic and failure characteristics of Bridgestone isolation bearings', *Report No. UCB/EERC 91/04*, Earthquake Engineering Research Center, University of California, Berkeley, 1991.
2. H. Ozdemir, 'Nonlinear transient dynamic analysis of yielding structures', *Ph.D. Dissertation*, Division of Structural Engineering and Structural Mechanics, Department of Civil Engineering, University of California, Berkeley, 1976.
3. Y. K. Wen, 'Method for random vibration of hysteretic systems', *J. eng. mech. ASCE* **102**, 249–263 (1976).
4. G. F. Demetriades, M. C. Constantinou and A. M. Reinhorn, 'Study of wire rope systems for seismic protection of equipment in buildings', *Technical Report NCEER-92-0012*, State University of New York at Buffalo, 1992.
5. P. C. Tsopelas, M. C. Constantinou and A. M. Reinhorn, '3D-BASIS-ME: Computer program for nonlinear dynamic analysis of seismically isolated single and multiple structures and liquid tanks', *Technical Report NCEER-94-0010*, State University of New York at Buffalo, 1994.
6. T. Fujita, S. Suzuki and S. Fujita, 'High damping rubber bearings for seismic isolation of buildings (1st report, hysteretic restoring force characteristics and analytical models)', *Trans. Japan soc. mech. eng.* **C56**, 658–666 (1990) (in Japanese).
7. E. Rosenblueth and I. Herrera, 'On a kind of hysteretic damping', *J. eng. mech. div. ASCE* **90**, 37–48 (1964).
8. N. Murota, K. Goda, S. Suzuki, C. Sudo and Y. Suizu, 'Recovery characteristics of dynamic properties of high damping rubber bearings', *Proc. 3rd U.S.–Japan workshop on earthquake protective systems for bridges*, Berkeley, pp. 63–76, 1994.
9. I. D. Aiken, J. M. Kelly, P. W. Clark, K. Tamura, M. Kikuchi and T. Itoh, 'Experimental studies of the mechanical characteristics of three types of seismic isolation bearings', *Proc. 10th world conf. on earthquake eng.* Vol. 4, Madrid, pp. 2281–2286, 1992a.
10. I. D. Aiken, P. W. Clark and J. M. Kelly, 'Mechanical characteristics of elastomeric seismic isolation bearings', *2nd U.S.–Japan joint workshop on earthquake protective systems for bridges*, Tsukuba, Japan, 1992b.
11. I. D. Aiken, P. W. Clark, J. M. Kelly, M. Kikuchi, M. Saruta and K. Tamura, 'Design- and ultimate-level earthquake tests of a 1/2·5-scale base-isolated reinforced-concrete building', *Proc. ATC-17-1 seminar on seismic isolation, passive energy dissipation, and active control*, vol. 1, San Francisco, pp. 281–292, 1993.
12. M. Watabe, J. Kanda, M. Yoshimura, A. Sato, T. Kaminaga and K. Saida, 'Seismic response of average high-rise building structures in Japan', *Proc. ASCE ann. meeting*, Los Angeles, pp. 1–6, 1993.
13. M. F. Giberson, 'Two nonlinear beams with definitions of ductility', *J. struct. div. ASCE* **95**, 137–157 (1969).
14. T. Takeda, M. A. Sozen and N. N. Nielsen, 'Reinforced concrete response to simulated earthquakes', *J. struct. div. ASCE* **96**, 2557–2573 (1970).
15. M. Kikuchi, S. Hayashi and H. Watanabe, 'Dynamic performance of a base-isolation system for seismic protection and vibration isolation', *J. struct. eng. AIJ* **41B**, 69–78 (1995) (in Japanese).